PERGAMON International Journal of Multiphase Flow 25 (1999) 683–704

International Journal of Multiphase Flow

Derivation of Forchheimer terms and their verification by application to waves propagation in porous media

A. Levy [a,*], D. Levi-Hevroni [a], S. Sorek [a,b], G. Ben-Dor [a]

[a] *Department of Mechanical Engineering, Pearlstone Center for Aeronautical Studies, Ben-Gurion University of the Negev, Beer Sheva, Israel*

[b] *J. Blaustein Institute for Desert Research, Water Resources Research Center, Ben-Gurion University of the Negev, Beer Sheva, Israel*

Received 1 July 1996; received in revised form 10 February 1998

Abstract

Forchheimer terms are developed for the macroscopic momentum and energy balance equations considering saturated thermoelastic porous media, and for the macroscopic momentum balance equations in the case of multiphase porous media. It is shown that these terms represent the exchange between the interacting phases at their common interface. Using these Forchheimer terms, a very good agreement was evident when the 1-D numerical simulation of the propagation of compaction waves in a saturated thermoelastic porous medium was compared with shock tube experiments.

Keywords: Saturated or multiphase porous media; Mass, momentum and energy balance equations; Forchheimer terms; Compaction and shock waves; 1-D numerical simulation; Shock tube experiments

1. Introduction

Macroscopic mass, momentum and energy balance equations for the fluid phase and the solid matrix were formulated on the basis of representative elementary volume (REV) concepts by Bear and Bachmat (1990). Based on these, Bear and Sorek (1990) developed the dominant macroscopic forms of the mass and momentum balance equations following an abrupt pressure impact in saturated porous materials under isothermal conditions. It was shown that during a certain time period due to the domination of momentum inertial terms, the fluid momentum balance equation conforms to nonlinear wave equations form. This initiated the establishment

* Corresponding author.

0301-9322/99/$ - see front matter
PII: S0301-9322(98)00031-7

of the macroscopic theoretical basis for wave motion in multiphase deformable porous media. Bear et al. (1992) and Sorek et al. (1992) elaborated on these for the case of thermoelastic porous media, describing the theoretical basis for obtaining displacement and shock waves, respectively.

These models, however, excluded the possibility of the exchange of inertia through the solid–fluid interface. Following Sorek et al. (1992), Levy et al. (1995) introduced additional Forchheimer terms and obtained a variety of nonlinear wave equation forms. These, together with the development of the evolving balance equations following an abrupt simultaneous change of the fluid temperature and pressure, are the major novel theoretical aspects with respect to Nikolaevskij (1990).

Olim et al. (1994) applied the continuum mixture theory to model the saturated porous medium as an interaction between fluid and dust particles. In the phases momentum balance equations, they replaced the drag force by Darcy–Forchheimer forces. They ,however, noted correctly that such an approach could be justified only for infinitely weak foams in which the internal stresses were negligibly small.

We mostly find in the literature (Hsu and Cheng, 1990; Nield, 1991, 1994) that the Forchheimer term is referred to as being a drag force. Hsu and Cheng (1990) based their development on drag coefficients which assumed specific forms so as to be analogous to empirical forms of Darcy and Forchheimer terms. Nield (1991, 1994) introduced integral expressions of the pressure gradient at the solid–fluid interface. This, without any mathematical development, was then referred to as being equivalent to the empirical forms of Darcy and Forchheimer terms. Mei and Auriault (1991) applied a perturbation method to the variations about the fluid velocities and its pressure; this, in reference to the microscopic steady state N.S. equations of the fluid momentum balance. As a result, they obtained balance equations valid for three different orders of magnitude. The results of the 2nd order incorporated velocities with a third power. This mathematical development has no physical ground. Forchheimer terms, however, incorporate 2nd power velocities and are in line with the inertial terms. A similar development was presented by Wodie and Levy (1991). Using the perturbation method, they arrived at a velocity with a fourth power which was claimed (without proof) to be canceled in the case of macroscopic isotropy. The final form, however, was with a velocity having a power of three. The perturbation method was also applied by Tiziana (1997). It was claimed that the Forchheimer terms were obtained from Brinkman's drag terms stipulating that the permeability tensor was a function of the fluid velocity. Whitaker (1996) obtained macroscopic momentum balance equations by averaging its micorscopic form. The author maintained that Forchheimer terms emerged from Brinkman's microscopic drag term being transfered through the common solid–fluid interface. He thus arrived at a form which involved the product between the fluid velocity and a gradient of a tensor which mapped the deviation of the velocity onto its average value. Not only did such a product not yield a square power for the velocities, but also it was stipulated (without proof) that this tensor was a function of the velocity terms.

Based on Levy et al. (1995) and Levy (1995), we will develop rigorous mathematical macroscopic expressions accounting for Forchheimer terms representing the microscopic inertial transfer through a common phases interface when describing the flow phenomenon in saturated and multiphase porous media. We will then show the significance of such terms by

comparing the 1-D numerical simulation of compaction waves propagating through a saturated thermoelastic porous medium with experimental observations.

2. Averaging rules

To demonstrate the averaging technique and the form of the macroscopic equations that they yield, we follow Bear and Bachmat (1990) for the case of a porous medium of general local geometry.

The average of an intensive variable, e_α, of the α-phase ($\alpha \equiv$ f, s where f denotes the fluid phase and s denotes the solid phase) within the REV is given by,

$$\overline{e_\alpha}^{\alpha} = \frac{1}{U_\alpha}\int_{U_0} e_\alpha \, \mathrm{d}U_0 \tag{1}$$

where U_o denotes the volume of the REV, and U_α denotes the volume of the α-phase within U_0. Corresponding averages are defined for time and space derivatives, taking into account both the changes in the averaged quantities $\overline{e_\alpha}^{\alpha}$ and the fluxes through the REV boundaries.

Average of a time derivative

$$\theta_\alpha \overline{\frac{\partial e}{\partial t}}^{\alpha} = \frac{\partial \theta_\alpha \overline{e}^{\alpha}}{\partial t} - \frac{1}{U_0}\int_{S_{\alpha s}} e\mathbf{u}\cdot\boldsymbol{\xi}\, \mathrm{d}s \tag{2}$$

where θ_α denotes the volumetric fraction of the α-phase within the REV, for saturated porous media, this equals the porosity ϕ (i.e. $\theta_f = \phi$). The interface between the α-phase and the solid phase ($\alpha \equiv$ s) is denoted by $S_{\alpha s}$, $\mathbf{u}$ denotes the velocity of the (possibly moving) α surface and $\boldsymbol{\xi}$ denotes a unit vector perpendicular to that interface.

Average of a spatial derivative

$$\theta_\alpha \overline{\frac{\partial e}{\partial x_i}}^{\alpha} = \frac{\partial \theta_\alpha \overline{e}^{\alpha}}{\partial x_i} + \frac{1}{U_0}\int_{S_{\alpha s}} e_\alpha \xi_i \, \mathrm{d}s. \tag{3}$$

A modified rule for averaging a spatial derivative

$$\overline{\frac{\partial e}{\partial x_i}}^{\alpha} = \frac{\partial \overline{e}^{\alpha}}{\partial x_j} T^*_{\alpha ij} + \frac{1}{\phi U_0}\int_{S_{\alpha s}} \overset{\circ}{x}_i \frac{\partial e}{\partial x_j}\xi_j \, \mathrm{d}s \tag{4}$$

where $\overset{\circ}{x}_i$ denotes the ith coordinate of a point in the REV relative to the REV's centroid. Bachmat and Bear (1986), assumed that the modified rule can be justified for the fluid pressure (P) for a case $\nabla^2 P = 0$. The tensorial tortuosity coefficient, $T^*_{\alpha ij}$, appearing in (4) is defined by

$$T^*_{\alpha ij} = \frac{1}{\phi U_0}\int_{S_{\alpha\alpha}} \overset{\circ}{x}_i \xi_j \, \mathrm{d}s \tag{5}$$

where $S_{\alpha\alpha}$ denotes the α–α part of the REV boundary. This macroscopic coefficient reflects the microscopic configuration of the solid–fluid interface.

3. Macroscopic balance equations

3.1. Saturated thermoelastic porous media

Bear and Bachmat (1990) applied averaging rules such as those given by equations (1)–(5) to the microscopic balance equations of both phases in a saturated porous medium to obtain the macroscopic balance equations for a compressible Newtonian fluid and a thermoelastic solid matrix. The phases macroscopic balance equations, neglecting their dispersive flux terms, read as follows.

3.1.1. Fluid mass balance equation

$$\frac{\partial}{\partial t}\phi\overline{\rho_{\mathrm{f}}}^{\mathrm{f}} = -\nabla\cdot\phi\overline{\rho_{\mathrm{f}}}^{\mathrm{f}}\overline{\mathbf{V}_{\mathrm{f}}}^{\mathrm{f}}. \tag{6}$$

3.1.2. Solid mass balance equation

$$\frac{\partial}{\partial t}(1-\phi)\overline{\rho_{\mathrm{s}}}^{\mathrm{s}} = -\nabla\cdot(1-\phi)\overline{\rho_{\mathrm{s}}}^{\mathrm{s}}\overline{\mathbf{V}_{\mathrm{s}}}^{\mathrm{s}}. \tag{7}$$

3.1.3. Fluid momentum balance equation

$$\begin{aligned}\phi\overline{\rho_{\mathrm{f}}}^{\mathrm{f}}\frac{\mathrm{D}_{\mathrm{f}}}{\mathrm{D}t}\overline{\mathbf{V}_{\mathrm{f}}}^{\mathrm{f}} = & -\phi\mathbf{T}_{\mathrm{f}}^{*}\nabla\overline{P}^{\mathrm{f}} - \frac{1}{U_0}\int_{S_{\mathrm{fs}}}\overset{\circ}{x}\nabla P\cdot\boldsymbol{\xi}\,\mathrm{d}S + \phi\overline{\rho_{\mathrm{f}}}^{\mathrm{f}}g\nabla Z \\ & + (\overline{\mu_{\mathrm{f}}}^{\mathrm{f}} + \overline{\lambda_{\mathrm{f}}''}^{\mathrm{f}})\{\nabla[\nabla\cdot\phi(\overline{\mathbf{V}_{\mathrm{f}}}^{\mathrm{f}} - \overline{\mathbf{V}_{\mathrm{s}}}^{\mathrm{s}})] + \nabla\phi\nabla\cdot\overline{\mathbf{V}_{\mathrm{s}}}^{\mathrm{s}}\} \\ & + \overline{\mu_{\mathrm{f}}}^{\mathrm{f}}[\nabla^2\phi(\overline{\mathbf{V}_{\mathrm{f}}}^{\mathrm{f}} - \overline{\mathbf{V}_{\mathrm{s}}}^{\mathrm{s}}) + \nabla\overline{\mathbf{V}_{\mathrm{s}}}^{\mathrm{s}}] - \overline{\mu_{\mathrm{f}}}^{\mathrm{f}}\frac{c_{\mathrm{f}}}{\nabla_{\mathrm{f}}^2}\phi(\overline{\mathbf{V}_{\mathrm{f}}}^{\mathrm{f}} - \overline{\mathbf{V}_{\mathrm{s}}}^{\mathrm{s}})\cdot\alpha\end{aligned} \tag{8}$$

where

$$\frac{\mathrm{D}_{\alpha}}{\mathrm{D}t} \equiv \frac{\partial}{\partial t} + \mathbf{V}_{\alpha}\cdot\nabla$$

denotes the material derivative, which expresses the rate of change from the point of view of an observer traveling at the velocity $\mathbf{V}_{\alpha}$ of the α phase, ρ_{α} denotes the density of the α phase,

$g\nabla Z$ denotes the gravity acceleration in the Z direction, $\overline{\mu_{\mathrm{f}}}^{\mathrm{f}}$ and $\overline{\lambda_{\mathrm{f}}''}^{\mathrm{f}}$ denote, respectively, the first and second fluid viscosities, c_{f} denotes a shape factor, α denotes a tensor associated with the matrix directional cosines and Δ_{f} denotes the hydraulic radius of the pore spaces.

3.1.4. Porous medium momentum balance equation

By summing the macroscopic momentum balance equations for the fluid and for the thermoelastic solid phases, the rate of momentum exchange across the solid–fluid interface is eliminated and we obtain the momentum balance equation for the porous medium as a whole in the form

$$\begin{aligned}\phi\overline{\rho_{\mathrm{f}}}^{\mathrm{f}}\frac{\mathrm{D_f}}{\mathrm{D}t}\overline{\mathbf{V}_{\mathrm{f}}}^{\mathrm{f}}+(1-\phi)\overline{\rho_{\mathrm{s}}}^{\mathrm{s}}\frac{\mathrm{D_s}}{\mathrm{D}t}\overline{\mathbf{V}_{\mathrm{s}}}^{\mathrm{s}} &= -[\phi\overline{\rho_{\mathrm{f}}}^{\mathrm{f}}+(1-\phi)\overline{\rho_{\mathrm{s}}}^{\mathrm{s}}]g\nabla Z\\ &\quad+\frac{\overline{\mu_{\mathrm{f}}}^{\mathrm{f}}}{\phi}[\nabla^2\phi(\overline{\mathbf{V}_{\mathrm{f}}}^{\mathrm{f}}-\overline{\mathbf{V}_{\mathrm{s}}}^{\mathrm{s}})+\nabla\nabla\cdot\phi(\overline{\mathbf{V}_{\mathrm{f}}}^{\mathrm{f}}-\overline{\mathbf{V}_{\mathrm{s}}}^{\mathrm{s}})]\\ &\quad+\frac{\overline{\lambda_{\mathrm{f}}''}^{\mathrm{f}}}{\phi}\nabla\nabla\cdot\phi(\overline{\mathbf{V}_{\mathrm{f}}}^{\mathrm{f}}-\overline{\mathbf{V}_{\mathrm{s}}}^{\mathrm{s}})+\overline{\mu_{\mathrm{f}}}^{\mathrm{f}}(\nabla^2\overline{\mathbf{V}_{\mathrm{s}}}^{\mathrm{s}}+\nabla\nabla\cdot\overline{\mathbf{V}_{\mathrm{s}}}^{\mathrm{s}})\\ &\quad+\overline{\lambda_{\mathrm{f}}''}^{\mathrm{f}}\nabla\nabla\cdot\overline{\mathbf{V}_{\mathrm{s}}}^{\mathrm{s}}-\nabla\overline{P}^{\mathrm{f}}-\bar{\eta}\nabla\overline{T_{\mathrm{S}}}^{\mathrm{s}}+\overline{\mu_{\mathrm{s}}'}^{\mathrm{s}}\nabla\cdot\boldsymbol{\varepsilon}_{\mathrm{sk}}+\overline{\lambda_{\mathrm{s}}''}^{\mathrm{s}}\nabla\varepsilon_{\mathrm{sk}}\end{aligned}\tag{9}$$

where $\mathbf{I}$ denotes a unit tensor, $\overline{T_\alpha}^{\alpha}$ denotes the α-phase temperature, $\overline{\mu_{\mathrm{s}}'}^{\mathrm{s}}$, $\overline{\lambda_{\mathrm{s}}''}^{\mathrm{s}}$ and $\bar{\eta}$ denote the Lame's constants for a thermoelastic solid matrix, $\boldsymbol{\varepsilon}_{\mathrm{sk}}$ and $\varepsilon_{\mathrm{sk}}$ denote its strain tensor and volumetric strain, respectively, and associated with $\mathbf{w}_{\mathrm{s}}$, its displacement vector, defined by

$$\boldsymbol{\varepsilon}_{\mathrm{sk}}=\tfrac{1}{2}[\nabla\mathbf{w}_{\mathrm{s}}+(\nabla\mathbf{w}_{\mathrm{s}})^{\mathrm{T}}],\tag{10}$$

$$\varepsilon_{\mathrm{sk}}=\nabla\cdot\mathbf{w}_{\mathrm{s}}.\tag{11}$$

In (9) we may introduce two new quantities, the bulk density, ρ_{b}, given by

$$\rho_{\mathrm{b}}\equiv\phi\overline{\rho_{\mathrm{f}}}^{\mathrm{f}}+(1-\phi)\overline{\rho_{\mathrm{s}}}^{\mathrm{s}}\tag{12}$$

and $\boldsymbol{\sigma}_{\mathrm{s}}'$, the effective stress tensor for the thermoelastic solid matrix which its constitutive relation reads,

$$\boldsymbol{\sigma}_{\mathrm{s}}'=\overline{\lambda_{\mathrm{s}}''}^{\mathrm{s}}\varepsilon_{\mathrm{sk}}\mathbf{I}+2\overline{\mu'}^{\mathrm{s}}\boldsymbol{\varepsilon}_{\mathrm{sk}}-\bar{\eta}(\overline{T_{\mathrm{s}}}^{\mathrm{s}}-\overline{T_{\mathrm{s}_0}}^{\mathrm{s}})\mathbf{I}.\tag{13}$$

In writing the macroscopic energy balance equations for the fluid and the solid phases, we assume linear thermodynamics, omit external energy sources and the energy associated with the fluid shear tensor $\boldsymbol{\tau}$ (viscous dissipation) is assumed negligible, i.e. $|\boldsymbol{\tau}:\nabla\mathbf{V}_{\mathrm{f}}|\ll|P\nabla\cdot\mathbf{V}_{\mathrm{f}}|$. We thus obtain the following.

3.1.5. Fluid energy balance equation

$$\frac{\partial}{\partial t}\left\{\phi\overline{\rho}_{\mathrm{f}}^{\mathrm{f}}\left[C_{\mathrm{f}}\overline{T}_{\mathrm{f}}^{\mathrm{f}}+\frac{(\overline{\mathbf{V}}_{\mathrm{f}}^{\mathrm{f}})^2}{2}\right]\right\}=-\alpha^{*\mathrm{H}}(\overline{T}_{\mathrm{f}}^{\mathrm{f}}-\overline{T}_{\mathrm{s}}^{\mathrm{s}})+\mathbf{T}_{\mathrm{s}}^{*}\overline{P}^{\mathrm{f}}\overline{\mathbf{V}}_{\mathrm{s}}^{\mathrm{s}}\cdot\nabla\phi$$
$$-\mathbf{T}_{\mathrm{f}}^{*}\nabla\cdot(\phi\overline{P}^{\mathrm{f}}\overline{\mathbf{V}}_{\mathrm{f}}^{\mathrm{f}})-\frac{1}{U_0}\int_{S_{\mathrm{fs}}}\mathring{x}\overline{\mathbf{V}}_{\mathrm{f}}^{\mathrm{f}}\nabla P\cdot\xi\,\mathrm{d}S$$
$$-\nabla\cdot\left\{\phi\overline{\rho}_{\mathrm{f}}^{\mathrm{f}}\left[C_{\mathrm{f}}\overline{T}_{\mathrm{f}}^{\mathrm{f}}+\frac{(\overline{\mathbf{V}}_{\mathrm{f}}^{\mathrm{f}})^2}{2}\right]\overline{\mathbf{V}}_{\mathrm{f}}^{\mathrm{f}}\right\}$$
$$+\nabla\cdot\{\phi\mathbf{D}^{*\mathrm{H}}\nabla(C_{\mathrm{f}}\overline{\rho}_{\mathrm{f}}^{\mathrm{f}}\overline{T}_{\mathrm{f}}^{\mathrm{f}})+\phi\overline{\lambda}_{\mathrm{f}}^{\mathrm{f}}\nabla\overline{T}_{\mathrm{f}}^{\mathrm{f}}\}\tag{14}$$

where C_α denotes the constant specific heat at constant volume for the fluid phase ($\alpha\equiv\mathrm{f}$) or at constant strain for a solid matrix ($\alpha\equiv\mathrm{s}$), $\overline{\lambda_\alpha}^{\alpha}$ denotes the thermal conductivity for the α-phase, $\alpha^{*\mathrm{H}}$ denotes the convection heat transfer coefficient and $\mathbf{D}^{*\mathrm{H}}$ denotes the dispersive heat tensor for the fluid.

3.1.6. Solid energy balance equation

$$\frac{\partial}{\partial t}\left\{(1-\phi)\overline{\rho}_{\mathrm{s}}^{\mathrm{s}}\left[C_{\mathrm{f}}\overline{T}_{\mathrm{s}}^{\mathrm{s}}+\frac{(\overline{\mathbf{V}}_{\mathrm{s}}^{\mathrm{s}})^2}{2}\right]\right\}=-\alpha^{*\mathrm{H}}(\overline{T}_{\mathrm{s}}^{\mathrm{s}}-\overline{T}_{\mathrm{f}}^{\mathrm{f}})-\mathbf{T}_{\mathrm{s}}^{*}\overline{P}^{\mathrm{f}}\overline{\mathbf{V}}_{\mathrm{s}}^{\mathrm{s}}\cdot\nabla\phi$$
$$+\mathbf{T}_{\mathrm{s}}^{*}\nabla\cdot[(1-\phi)\overline{P}^{\mathrm{f}}\overline{\mathbf{V}}_{\mathrm{s}}^{\mathrm{s}}]+\frac{1}{U_0}\int_{S_{\mathrm{fs}}}\mathring{x}\,\overline{\mathbf{V}}_{\mathrm{f}}^{\mathrm{f}}\nabla P\cdot\boldsymbol{\xi}\,\mathrm{d}S-\nabla\cdot(\boldsymbol{\sigma}_{\mathrm{s}}'\overline{\mathbf{V}}^{\mathrm{s}})$$
$$-\nabla\cdot\left\{(1-\phi)\overline{\rho}_{\mathrm{s}}^{\mathrm{s}}\left[C_{\mathrm{s}}\overline{T}_{\mathrm{s}}^{\mathrm{s}}+\frac{(\overline{\mathbf{V}}_{\mathrm{s}}^{\mathrm{s}})^2}{2}\right]\overline{\mathbf{V}}_{\mathrm{s}}^{\mathrm{s}}-(1-\phi)\overline{\lambda}_{\mathrm{s}}^{\mathrm{s}}\nabla\overline{T}_{\mathrm{s}}^{\mathrm{s}}\right\}.\tag{15}$$

3.1.7. Mathematical derivation of Forchheimer terms

In order to calculate the integrals appearing in equations (8), (14) and (15), Bear and Bachmat (1990) assumed that the microscopic drag (associated with the shear stress tensor $\tau_{\mathrm{f}_{ij}}$ of the Newtonian fluid) and inertial forces at the solid–fluid interface are much smaller than the surface and body (gravity) forces, i.e.

$$\left|\left(\rho_{\mathrm{f}}\frac{\partial V_{\mathrm{f}_j}}{\partial t}+\rho_{\mathrm{f}}V_{\mathrm{f}_i}\frac{\partial V_{\mathrm{f}_j}}{\partial x_i}-\frac{\partial\tau_{\mathrm{f}_{ij}}}{\partial x_i}\right)\xi_j\right|\ll\left|\left(\frac{\partial P}{\partial x_j}+\rho_{\mathrm{f}}g\frac{\partial Z}{\partial x_j}\right)\xi_j\right|.\tag{16}$$

Using (16) they calculated the integral in (8) and obtained a macroscopic term in the form,

$$\frac{1}{U_0}\int_{S_{\mathrm{fs}}} \overset{\circ}{x}\,\nabla P\cdot\boldsymbol{\xi}\,\mathrm{d}S = -\phi\overline{\rho_{\mathrm{f}}}^{\mathrm{f}} g(\nabla Z)^{\mathrm{T}}(\mathbf{I}-\mathbf{T}_{\mathrm{f}}^{*}) \tag{17}$$

where $(\,)^{\mathrm{T}}$ denotes the transpose of a vector.

For high fluid velocities, we suggest to include an inertial term to the RHS of (16) to read,

$$\left|\left(\rho_{\mathrm{f}}\frac{\partial V_{\mathrm{f}_j}}{\partial t}-\frac{\partial \tau_{\mathrm{f}_{ij}}}{\partial x_i}\right)\xi_j\right| \ll \left|\left(\frac{\partial P}{\partial x_j}+\rho_{\mathrm{f}} g\frac{\partial Z}{\partial x_j}+\rho_{\mathrm{f}} V_{\mathrm{f}_i}\frac{\partial V_{\mathrm{f}_j}}{\partial x_i}\right)\xi_j\right|. \tag{18}$$

In view of (18), at the solid–fluid interface (S_{fs}), we may assume

$$\frac{\partial P}{\partial x_j}\xi_j \cong -\left(\rho_{\mathrm{f}} g\frac{\partial Z}{\partial x_j}+\rho_{\mathrm{f}} V_{\mathrm{f}_i}\frac{\partial V_{\mathrm{f}_f}}{\partial x_i}\right)\xi_j. \tag{19}$$

Integration over S_{fs} of the first term on the RHS of (19), will yield the RHS term as in (17). However, integration over S_{fs} of the second term on the RHS of (19) will read,

$$\begin{aligned}
&-\frac{1}{U_0}\int_{S_{\mathrm{fs}}} \overset{\circ}{x}_i\rho_{\mathrm{f}} V_{\mathrm{f}_k}\frac{\partial V_{\mathrm{f}_j}}{\partial x_k}\xi_j\,\mathrm{d}S \\
&= \frac{1}{U_0}\int_{S_{\mathrm{fs}}} \overset{\circ}{x}_i\rho_{\mathrm{f}}\left[-\frac{1}{2}\frac{\partial}{\partial x_j}(V_{\mathrm{f}_k}V_{\mathrm{f}_k})+V_{\mathrm{f}_k}\left(\frac{\partial V_{\mathrm{f}_k}}{\partial x_j}-\frac{\partial V_{\mathrm{f}_j}}{\partial x_k}\right)\right]\xi_j\,\mathrm{d}S.
\end{aligned} \tag{20}$$

We now refer to (2.6.33)–(2.6.39) in Bear and Bachmat (1990). We assume no slip conditions at the solid–fluid interface as well as being material at the microscopic level. By virtue of the integral form of the mean value theorem, we also assume that there exist mean values for the velocities of the RHS integral of (20). Hence, the first RHS integral of (20) can be approximated by

$$\begin{aligned}
&\frac{1}{U_0}\int_{S_{\mathrm{fs}}} \overset{\circ}{x}_i\rho_{\mathrm{f}}\left[-\frac{1}{2}\frac{\partial}{\partial x_j}(V_{\mathrm{f}_k}V_{\mathrm{f}_k})\right]\xi_j\,\mathrm{d}S \\
&\cong -\frac{1}{2U_0}\int_{S_{\mathrm{fs}}} \overset{\circ}{x}_i\rho_{\mathrm{f}}\frac{(V_{\mathrm{s}_k}V_{\mathrm{s}_k}-V_{\mathrm{f}_k}V_{\mathrm{f}_k})}{\Delta}\xi_j\,\mathrm{d}S \\
&= -\frac{1}{2U_0}\int_{S_{\mathrm{fs}}} \overset{\circ}{x}_i\rho_{\mathrm{f}}\frac{(\overline{V_{\mathrm{s}_k}}^{\mathrm{s}}+\overline{V_{\mathrm{f}_n}}^{\mathrm{f}})(\overline{V_{\mathrm{s}_j}}^{\mathrm{s}}-\overline{V_{\mathrm{f}_j}}^{\mathrm{f}})}{\Delta}(\delta_{jk}-\xi_j\xi_k)\,\mathrm{d}S \\
&\cong \frac{c_{\mathrm{f}}}{2\Delta_{\mathrm{f}}^2}\phi\overline{\rho_{\mathrm{f}}}^{\mathrm{f}}\tilde{F}_{ijk}(\overline{V_{\mathrm{s}_k}}^{\mathrm{s}}+\overline{V_{\mathrm{f}_k}}^{\mathrm{f}})V_{\mathrm{r}_j}
\end{aligned} \tag{21}$$

where Δ denotes a characteristic distance from the solid surface to the fluid within the pore space, δ_{jk} denotes the components of the Kronecker delta function and $\mathbf{V}_{\mathrm{r}}$ ($\equiv\overline{\mathbf{V}}_{\mathrm{f}}^{\mathrm{f}}-\overline{\mathbf{V}}_{\mathrm{s}}^{\mathrm{s}}$) denotes a relative velocity vector. We note that, Δ_{f} ($\equiv U_{0\mathrm{f}}/S_{\mathrm{fS}}$), the fluid hydraulic radius of the pore spaces is also related to $c_{\mathrm{f}}\Delta$. The components of the third rank tensor $\tilde{F}_{ijk}$ is associated with the matrix of directional cosines and the $\overset{\circ}{x}$ vector

$$\tilde{F}_{ijk} \equiv \frac{1}{S_{\mathrm{fs}}} \int_{S_{\mathrm{fs}}} \overset{\circ}{x}_i (\delta_{jk} - \xi_j \xi_k)\, \mathrm{d}S. \tag{22}$$

Similarly as in (21), we approximate the first part of the second RHS integral of (20) to read

$$\frac{1}{U_0} \int_{S_{\mathrm{fs}}} \overset{\circ}{x}_i \rho_{\mathrm{f}} \left[V_{\mathrm{f}_k} \frac{\partial V_{\mathrm{f}_k}}{\partial x_j} \right] \xi_j \, \mathrm{d}S \cong \frac{c_{\mathrm{f}}}{\Delta_{\mathrm{f}}^2} \phi \overline{\rho_{\mathrm{f}}}^{\mathrm{f}} \tilde{F}_{ijk} \overline{V_{\mathrm{s}_k}}^{\mathrm{s}} V_{\mathrm{r}_j}. \tag{23}$$

To approximate the second part of the second RHS integral of (20), we also make use of (4) and (5). We thus obtain

$$\frac{1}{U_0} \int_{S_{\mathrm{fs}}} \overset{\circ}{x}_i \rho_{\mathrm{f}} \left[-V_{\mathrm{f}_k} \frac{\partial V_{\mathrm{f}_j}}{\partial x_k} \right] \xi_j \, \mathrm{d}S \cong -\phi \overline{\rho_{\mathrm{f}}}^{\mathrm{f}} \overline{V_{\mathrm{s}_k}}^{\mathrm{s}} \frac{\overline{\partial V_{\mathrm{f}_j}}^{\mathrm{f}}}{\partial x_k} (\delta_{ij} - T^*_{\mathrm{f}_{ij}}). \tag{24}$$

Furthermore, by virtue of (3), we write

$$\begin{aligned} \phi \frac{\overline{\partial V_{\mathrm{f}_j}}^{\mathrm{f}}}{\partial x_k} &= \frac{\partial}{\partial x_k} (\phi \overline{V_{\mathrm{f}_j}}^{\mathrm{f}}) + \frac{1}{U_0} \int_{S_{\mathrm{fs}}} V_{\mathrm{f}_j} \xi_j \, \mathrm{d}S \\ &= \frac{\partial}{\partial x_k} (\phi \overline{V_{\mathrm{f}_j}}^{\mathrm{f}}) + \left[-\frac{\partial}{\partial x_k} (\phi \overline{V_{\mathrm{s}_j}}^{\mathrm{s}}) + \phi \frac{\partial \overline{V_{\mathrm{s}_j}}^{\mathrm{s}}}{\partial x_k} \right] \\ &= \frac{\partial}{\partial x_k} (\phi V_{\mathrm{r}_j}) + \phi \frac{\partial \overline{V_{\mathrm{s}_j}}^{\mathrm{s}}}{\partial x_k}. \end{aligned} \tag{25}$$

Combining (21) and (23) to (25), we write (20) in the form,

$$\begin{aligned} -\frac{1}{U_0} \int_{S_{\mathrm{fs}}} \overset{\circ}{x}_i \rho_{\mathrm{f}} V_{\mathrm{f}_k} \frac{\partial V_{\mathrm{f}_j}}{\partial x_k} \xi_j \, \mathrm{d}S = \frac{c_{\mathrm{f}}}{2\Delta_{\mathrm{f}}^2} \phi \overline{\rho_{\mathrm{f}}}^{\mathrm{f}} \tilde{F}_{ijk} V_{\mathrm{r}_j} V_{\mathrm{r}_k} \\ - \overline{\rho_{\mathrm{f}}}^{\mathrm{f}} \overline{V_{\mathrm{s}_k}}^{\mathrm{s}} \left[\frac{\partial}{\partial x_k} (\phi V_{\mathrm{r}_j}) + \phi \frac{\partial \overline{V_{\mathrm{s}_j}}^{\mathrm{s}}}{\partial x_k} \right] (\delta_{ij} - T^*_{\mathrm{f}_{ij}}). \end{aligned} \tag{26}$$

We note that the RHS of (26) can be neglected when $\overline{\mathbf{V}_{\mathrm{s}}}^{\mathrm{s}} \ll \overline{\mathbf{V}_{\mathrm{f}}}^{\mathrm{f}}$.

3.2. Multiphase porous media

Consider the mutual interactions between two fluid phases denoted by subscript $(\,)_\beta$ with, say, $\beta \equiv \ell$ for the liquid phase, $\beta \equiv g$ for the gas phase and subscript $(\,)_\alpha$ for $\alpha \equiv \mathrm{s}$ the solid phase. Let us assume Newtonian fluids, isentropic conditions, incompressible solid and a deformable matrix, the solid–fluids interfaces $S_{\mathrm{s}\beta}$ are subject to no slip conditions as well as being material at the microscopic level, while the liquid–gas interface is assumed to be not material at that level. We modify the macroscopic balance equations appearing in Bear and Bachmat (1990) to read as follows.

3.2.1. Liquid mass balance equation

$$\frac{\partial}{\partial t}(\theta_\ell \overline{\rho_\ell}^{\ell}) = -\nabla \cdot (\theta_\ell \overline{\rho_\ell}^{\ell} \overline{\mathbf{V}_\ell}^{\ell}) - \frac{1}{U_o}\int_{S_{\ell g}} \rho_\ell (\mathbf{V}_\ell - \mathbf{u}) \cdot \boldsymbol{\xi}_\ell \, \mathrm{d}S. \tag{27}$$

3.2.2. Gas mass balance equation

$$\frac{\partial}{\partial t}(\theta_{\mathrm{g}} \overline{\rho_{\mathrm{g}}}^{\mathrm{g}}) = -\nabla \cdot (\theta_{\mathrm{g}} \overline{\rho_{\mathrm{g}}}^{\mathrm{g}} \overline{\mathbf{V}_{\mathrm{g}}}^{\mathrm{g}}) - \frac{1}{U_{\mathrm{o}}}\int_{S_{\ell g}} \rho_{\mathrm{g}} (\mathbf{V}_{\mathrm{g}} - \mathbf{u}) \cdot \boldsymbol{\xi}_{\mathrm{g}} \, \mathrm{d}S \tag{28}$$

where s_ℓ denotes the storativity of the liquid phase, θ_β ($\beta \equiv \ell$, g) and θ_{s} denotes the fluids and solid volume fractions respectively, given by,

$$\theta_\ell = s_\ell \phi,$$

$$\theta_{\mathrm{g}} = (1 - s_\ell)\phi,$$

$$\theta_{\mathrm{s}} = (1 - \phi). \tag{29}$$

3.2.3. Solid mass balance equation

$$\frac{\partial}{\partial t}(\theta_{\mathrm{s}} \overline{\rho_{\mathrm{s}}}^{\mathrm{s}}) = -\nabla \cdot (\theta_{\mathrm{s}} \overline{\rho_{\mathrm{s}}}^{\mathrm{s}} \overline{\mathbf{V}_{\mathrm{s}}}^{\mathrm{s}}). \tag{30}$$

3.2.4. Liquid momentum balance equation

$$\begin{aligned}
\theta_\ell \overline{\rho_\ell}^{\ell} \frac{\mathrm{D}_\ell \overline{\mathbf{V}_\ell}^{\ell}}{\mathrm{D}t} = & -\theta_\ell \mathbf{T}_\ell^* \nabla \overline{P_\ell}^{\ell} - \frac{1}{U_{\mathrm{o}}}\int_{S_{\ell s}+S_{\ell g}} \mathring{x} \nabla P_\ell \cdot \boldsymbol{\xi}_\ell \, \mathrm{d}S + \theta_\ell \overline{\rho_\ell}^{\ell} g \nabla Z \\
& + (\overline{\mu_\ell}^{\ell} + \overline{\lambda_\ell''}^{\ell}) \nabla \nabla \cdot (\theta_\ell \overline{\mathbf{V}}_\ell^{\ell}) + \overline{\mu_\ell}^{\ell} \nabla^2 (\theta_\ell \overline{\mathbf{V}}_\ell^{\ell}) \\
& + (\overline{\mu_\ell}^{\ell} + \overline{\lambda_\ell''}^{\ell}) \left[\nabla \left(\frac{1}{U_0}\int_{S_{\ell s}+S_{\ell g}} \mathbf{V}_\ell \cdot \boldsymbol{\xi}_\ell \, \mathrm{d}S \right) + \frac{1}{U_{\mathrm{o}}}\int_{S_{\ell s}+S_{\ell g}} \nabla \cdot \mathbf{V}_\ell \boldsymbol{\xi}_\ell \, \mathrm{d}S \right] \\
& + \overline{\mu_\ell}^{\ell} \left[\nabla \cdot \left(\frac{1}{U_{\mathrm{o}}}\int_{S_{\ell s}+S_{\ell g}} \mathbf{V}_\ell \boldsymbol{\xi}_\ell \, \mathrm{d}S \right) + \frac{1}{U_{\mathrm{o}}}\int_{S_{\ell s}+S_{\ell g}} \nabla \mathbf{V}_\ell \cdot \boldsymbol{\xi}_\ell \, \mathrm{d}S \right].
\end{aligned} \tag{31}$$

3.2.5. Gas momentum balance equation

$$\theta_g\overline{\rho_g}^g\frac{D_g\overline{\mathbf{V}_g}^g}{Dt} = -\theta_g\mathbf{T}_g^*\nabla\overline{P_g}^g - \frac{1}{U_0}\int_{S_{gs}+S_{\ell g}}\overset{\circ}{x}\nabla P_g\cdot\boldsymbol{\xi}_g\,dS + \theta_g\overline{\rho_g}^g\,g\nabla Z$$
$$+(\overline{\mu_g}^g+\overline{\lambda''}^g)\nabla\nabla\cdot(\theta_g\overline{\mathbf{V}_g}^g)+\overline{\mu_g}^g\nabla^2(\theta_g\overline{\mathbf{V}_g}^g)$$
$$+(\overline{\mu_g}^g+\overline{\lambda''_g}^g)\left[\nabla\left(\frac{1}{U_0}\int_{S_{gs}+S_{\ell g}}\mathbf{V}_g\cdot\boldsymbol{\xi}_g\,dS\right)+\frac{1}{U_0}\int_{S_{sg}+S_{\ell g}}\nabla\cdot\mathbf{V}_g\boldsymbol{\xi}_g\,dS\right.$$
$$\left.+\overline{\mu_g}^g\left[\nabla\cdot\left(\frac{1}{U_0}\int_{S_{gs}+S_{\ell g}}\mathbf{V}_g\boldsymbol{\xi}_g\,dS\right)+\frac{1}{U_0}\int_{S_{gs}+S_{\ell g}}\nabla\mathbf{V}_g\cdot\boldsymbol{\xi}_g\,dS\right]\right]. \tag{32}$$

Note that in (31) and (32) we neglect the sources of moment associated with the transfer of mass through the liquid–gas interface.

3.2.6. Porous medium momentum balance equation

$$\theta_s\overline{\rho_s}^s\frac{D_s\overline{\mathbf{V}_s}^s}{Dt}+\theta_\ell\overline{\rho_\ell}^\ell\frac{D_\ell\overline{\mathbf{V}_\ell}^\ell}{Dt}+\theta_g\overline{\rho_g}^g\frac{D_g\overline{\mathbf{V}_g}^g}{Dt} = -(\theta_s\overline{\rho_s}^s+\theta_\ell\overline{\rho_\ell}^\ell+\theta_g\overline{\rho_g}^g)g\nabla Z$$
$$+(\overline{\mu_\ell}^\ell+\overline{\lambda''_\ell}^\ell)\nabla\nabla\cdot(\theta_\ell\overline{\mathbf{V}_\ell}^\ell)+\frac{\overline{\mu_\ell}^\ell}{\phi}\nabla^2(\theta_\ell\overline{\mathbf{V}_\ell}^\ell)-s_\ell\nabla P_\ell$$
$$+\frac{(\overline{\mu_g}^g+\overline{\lambda''_g}^g)}{\phi}\nabla\nabla\cdot(\theta_g\overline{\mathbf{V}_g}^g)+\frac{\overline{\mu_g}^g}{\phi}\nabla^2(\theta_g\overline{\mathbf{V}_g}^g)-(1-s_\ell)\nabla P_g$$
$$+\frac{1}{U_0}\int_{S_{\ell g}}(\boldsymbol{\sigma}_\ell-\boldsymbol{\sigma}_g)\cdot\boldsymbol{\xi}_\ell\,dS+\overline{\mu'_s}^s\nabla\cdot\boldsymbol{\varepsilon}_{sk}+\overline{\lambda''_s}^s\nabla\varepsilon_{sk}$$
$$+(\overline{\mu_\ell}^\ell+\overline{\lambda''_\ell}^\ell)\nabla\left(\frac{1}{U_0}\int_{S_{\ell s}+S_{\ell g}}\mathbf{V}_\ell\cdot\boldsymbol{\xi}_\ell\,dS\right)+\overline{\mu_\ell}^\ell\nabla\cdot\left(\frac{1}{U_0}\int_{S_{\ell s}+S_{\ell g}}\mathbf{V}_\ell\boldsymbol{\xi}_\ell\,dS\right)$$
$$+(\overline{\mu_g}^g+\overline{\lambda''_g}^g\nabla\left(\frac{1}{U_0}\int_{S_{gs}+S_{\ell g}}\mathbf{V}_g\cdot\boldsymbol{\xi}_g\,dS\right)+\overline{\mu_g}^g\nabla\cdot\left(\frac{1}{U}\int_{S_{gs}+S_{\ell g}}\mathbf{V}_g\boldsymbol{\xi}_g\,dS\right) \tag{33}$$

where $\boldsymbol{\sigma}_\beta$ denotes the microscopic stress tensor of the β, ($\equiv \ell$, g) fluid. We note that (33) is the macroscopic form of the porous medium as a whole and does not represent the summation of (31) and (32). Note also that the second line in the RHS of (33) accounts for the liquid macroscopic stress, while the third RHS line accounts for the gas macroscopic stress.

The exchange terms at the phases interfaces still need to be addressed. In, e.g. (27) for ϱ components being transfered from the liquid phase to the gas phase, Bear and Bachmat (1990) suggest a constitutive expression in the form,

$$\frac{1}{U_0}\int_{S_{\ell g}} \rho_\ell(\mathbf{V}_\ell - \mathbf{u})\cdot\boldsymbol{\xi}_\ell \, \mathrm{d}S = \sum_{\rho} \alpha^{*\varrho}(\overline{\rho_\ell^{\varrho}}^{\ell} - \overline{\rho_{\mathrm{g}}^{\varrho}}^{\mathrm{g}}) \tag{34}$$

in which $\alpha^{*\varrho}$ denotes a transfer coefficient and ρ_β^ϱ denotes the density of the ϱ component in the β fluid so that,

$$\rho_\beta = \sum_{\varrho} \rho_\beta^\varrho. \tag{35}$$

Since the liquid–gas interface is assumed to be non-material, the terms associated with the transfer of momentum between the fluid phases in (31), (32) and (33) read,

$$\frac{1}{U_0}\int_{S_{s\beta}+S_{\ell g}} \mathbf{V}_\beta\cdot\boldsymbol{\xi}_\beta \, \mathrm{d}S \cong \overline{\mathbf{V}_{\mathrm{s}}}^{\mathrm{s}}\cdot\nabla\theta_\beta + \frac{1}{U_0}\int_{S_{\ell g}} (\mathbf{V}_\beta - \overline{\mathbf{V}_{\mathrm{s}}}^{\mathrm{s}})\cdot\boldsymbol{\xi}_\beta \, \mathrm{d}S, \tag{36}$$

$$\frac{1}{U_0}\int_{S_{s\beta}+S_{\ell g}} \mathbf{V}_\beta\boldsymbol{\xi}_\beta \, \mathrm{d}S \cong \overline{\mathbf{V}_{\mathrm{s}}}^{\mathrm{s}}\nabla\theta_\beta + \frac{1}{U_0}\int_{S_{\ell g}} (\mathbf{V}_\beta - \overline{\mathbf{V}_{\mathrm{s}}}^{\mathrm{s}})\boldsymbol{\xi}_\beta \, \mathrm{d}S, \tag{37}$$

$$\frac{1}{U_0}\int_{S_{s\beta}+S_{\ell g}} \nabla\cdot\mathbf{V}_\beta\boldsymbol{\xi}_\beta \, \mathrm{d}S \cong -\overline{\nabla\cdot\mathbf{V}_\beta}^{\beta}\nabla\theta_\beta, \tag{38}$$

$$\frac{1}{U_0}\int_{S_{s\beta}+S_{\ell g}} \nabla\mathbf{V}_\beta\cdot\boldsymbol{\xi}_\beta \, \mathrm{d}S \cong -\frac{c_{s\beta}}{\Delta_{s\beta}^2}\boldsymbol{\alpha}\cdot\overline{\mathbf{V}_\beta}^{\beta} - \frac{c_{\ell g}}{\Delta_{\ell g}^2}\boldsymbol{\alpha}\cdot\left(\overline{\mathbf{V}_\beta}^{\beta} - \frac{1}{S_{\ell g}}\int_{S_{\ell g}} \mathbf{u}\, \mathrm{d}S\right) \tag{39}$$

where $c_{s\beta}$ denotes a shape factor associated with the β fluid at the $S_{s\beta}$ interface, $c_{\ell g}$ denotes a shape factor of the liquid and gas fluids at their $S_{\ell g}$ interface, $\Delta_{s\beta}$ and $\Delta_{\ell g}$ denote the hydraulic radius of the pore spaces associated with the $S_{s\beta}$ and $S_{\ell g}$ interfaces, respectively, defined by,

$$\Delta_{s\beta} \equiv U_{0\beta}/S_{s\beta}, \Delta_{\ell g} \equiv U_{s\beta}/S_{\ell g}. \tag{40}$$

The estimate of the integral expressions in the RHS of (36), (37) and (39) will be reported in the future. In the following we will present a rigorous mathematical evaluation of the integral expression in (31) and (32) leading to the Darcy and Forchheimer terms.

3.2.7. Mathematical derivation of Forchheimer terms

Basically, to a certain extent, we follow the same procedure as in the case of the saturated porous medium. With multi-fluids on hand we will, however, elaborate on the mathematical derivations. As in Bear and Bachmat (1990) we assume that the microscopic drag and inertial forces for the β ($\equiv \ell$, g) fluids at the gas–liquid interface are much smaller than those of the surface and body (gravity) forces, i.e.

$$\left|\left(\rho_\beta\frac{\partial V_{\beta_j}}{\partial t} + \rho_\beta V_{\beta_i}\frac{\partial V_{\beta_j}}{\partial x_i} - \frac{\partial\tau_{\beta_{ij}}}{\partial x_i}\right)\xi_j\right| \ll \left|\left(\frac{\partial P_\beta}{\partial x_j} + \rho_\beta g\frac{\partial Z}{\partial x_j}\right)\xi_j\right|. \tag{41}$$

Unlike Bear and Bachmat (1990), similar to (18) at the solid–fluid ($S_{s\beta}$) interfaces, assuming high fluid velocity in comparison to that of the solid, the following conditions will prevail,

$$\left|\left(\rho_\beta \frac{\partial V_{\beta_j}}{\partial t} - \frac{\partial \tau_{\beta_{ij}}}{\partial x_i}\right)\xi_j\right| \ll \left|\left(\frac{\partial P_\beta}{\partial x_j} + \rho_\beta g \frac{\partial Z}{\partial x_j} + \rho_\beta V_{\beta_i}\frac{\partial V_{\beta_j}}{\partial x_i}\right)\xi_j\right|. \tag{42}$$

Hence, in view of (42), at the $S_{S\beta}$ interfaces we may assume,

$$\frac{\partial P_\beta}{\partial x_j}\xi_j \cong -\left(\rho_\beta g \frac{\partial Z}{\partial x_j} + \rho_\beta V_{\beta_i}\frac{\partial V_{\beta_j}}{\partial x_i}\right)\xi_j. \tag{43}$$

In view of (41) and (42), the integration of (43) over the ($S_{s\beta} + S_{\ell g}$) interfaces reads,

$$\begin{aligned}\frac{1}{U_0}\int_{S_{s\beta}+S_{\ell g}} \mathring{x}_i \frac{\partial P_\beta}{\partial x_j}\xi_{\beta_j}\,\mathrm{d}S &\cong -\overline{\rho_\beta}^{\beta}\, g\delta_{3j}\frac{1}{U_0}\int_{S_{s\beta}+S_{\ell g}} \mathring{x}_i\xi_{\beta_j}\,\mathrm{d}S - \frac{1}{U_0}\int \mathring{x}_i\rho_\beta V_{\beta_k}\frac{\partial V_{\beta_j}}{\partial x_k}\xi_{\beta_j}\,\mathrm{d}S \\ &= -\theta_\beta\overline{\rho_\beta}^{\beta}\, g(\delta_{3j} - T^*_{\beta_{3i}}) - \frac{1}{U_o}\int_{S_{s\beta}} \mathring{x}_i\rho_\beta V_{\beta_k}\frac{\partial V_{\beta_j}}{\partial x_k}\xi_{\beta_j}\,\mathrm{d}S\end{aligned} \tag{44}$$

in which, by following Bear and Bachmat (1990) we write,

$$\frac{1}{U_0}\int_{S_{s\beta}+S_{\ell g}+S_{\beta\beta}} \mathring{x}_i\xi_{\beta_j}\,\mathrm{d}S = \delta_{ij}. \tag{45}$$

The integration appearing in (44) over the $S_{s\beta}$ interface can be rewritten in the form,

$$\begin{aligned}&-\frac{1}{U_0}\int_{S_{s\beta}} \mathring{x}_i\rho_\beta V_{\beta_k}\frac{\partial V_{\beta_j}}{\partial x_k}\xi_{\beta_j}\,\mathrm{d}S \\ &= \frac{1}{U_0}\int_{S_{s\beta}} \mathring{x}_i\rho_\beta\left[-\frac{1}{2}\frac{\partial}{\partial x_j}(V_{\beta_k}V_{\beta_k}) + V_{\beta_k}\left(\frac{\partial V_{\beta_k}}{\partial x_j} - \frac{\partial V_{\beta_j}}{\partial x_k}\right)\right]\xi_{\beta_j}\,\mathrm{d}S.\end{aligned} \tag{46}$$

The first term of the RHS integral of (46) can be estimated at the $S_{s\beta}$ interfaces by,

$$\frac{\partial}{\partial x_j}(V_{\beta_k}V_{\beta_k})\xi_{\beta_j}\bigg|_{S_{s\beta}} \cong \frac{V_{s_k}V_{s_k} - V_{\beta_k}V_{\beta_k}}{\Delta^c_{s\beta}}\bigg|_{S_{s\beta}} = \frac{(V_{s_k}+V_{\beta_k})(V_{s_j}-V_{\beta_j})}{\Delta^c_{s\beta}}(\delta_{kj} - \xi_{\beta_k}\xi_{\beta_j}) \tag{47}$$

where $\Delta^c_{s\beta}$ denotes a characteristic distance from the solid surface to each β fluid within the pore space. In view of (47), we estimate the first RHS integral of (46) to read,

$$\begin{aligned}&-\frac{1}{2U_0}\int_{S_{s\beta}} \mathring{x}_i\rho_\beta\frac{\partial}{\partial x_j}(V_{\beta_k}V_{\beta_k})\xi_{\beta_j}\,\mathrm{d}S \\ &\cong -\frac{1}{2U_0}\int_{S_s\beta} \mathring{x}_i\rho_\beta\frac{(V_{s_k}+V_{\beta_k})(V_{s_j}-V_{\beta_j})}{\Delta^c_{s\beta}}(\delta_{kj} - \xi_{\beta_k}\xi_{\beta_j})\,\mathrm{d}S \\ &\cong \frac{c_{s\beta}}{2\Delta^2_{s\beta}}\theta_\beta\overline{\rho_\beta}^{\beta}\tilde{F}^{s\beta}_{ijk}(\overline{V_{s_k}}^{s} + \overline{V_{\beta_k}}^{\beta})V_{r\beta_j}\end{aligned} \tag{48}$$

where $c_{s\beta}$, $\Delta^{c}_{s\beta}$ and $\Delta_{s\beta}$ are related by,

$$\Delta_{s\beta} = c_{s\beta}\Delta^{c}_{s\beta}; \tag{49}$$

the relative velocity vector between the β fluid phase and the solid phase is denoted by $\mathbf{V}_{r\beta}$ ($\equiv \overline{\mathbf{V}}^{f}_{\beta} - \overline{\mathbf{V}}^{s}_{s}$) and $\tilde{F}^{s\beta}_{ijk}$ denotes the components of the Forchheimer third rank tensor associated with the β fluid at the $S_{s\beta}$ interface, given by,

$$\tilde{F}^{s_\beta}_{ijk} \equiv \frac{1}{S_{s\beta}} \int_{S_{s\beta}} \overset{\circ}{x}_i (\delta_{kj} - \xi_{\beta_k}\xi_{\beta_j})\, \mathrm{d}S. \tag{50}$$

In writing the second RHS expression of (48), we made use of the integral form of the mean value theorem.

The second RHS integral of (46) is similarly estimated to read,

$$\frac{1}{U_0}\int_{S_s\beta} \overset{\circ}{x}_i \rho_\beta V_{\beta_k}\left(\frac{\partial V_{\beta_k}}{\partial x_j} - \frac{\partial V_{\beta_j}}{\partial x_i}\right)\xi_{\beta_j}\, \mathrm{d}S$$

$$\cong -\frac{c_\beta}{\Delta^2_\beta}\theta_\beta \overline{\rho_\beta}^{\beta}\tilde{F}^{s\beta}_{ijk}\overline{V_{s_k}}^{s} V_{r\beta_j} - \theta_\beta \overline{\rho_\beta}^{\beta}\,\overline{V_{s_k}}^{s}\,\overline{\frac{\partial V_{\beta_j}}{\partial x_k}}^{\beta}(\delta_{ij} - T^{*}_{\beta_{ij}}). \tag{51}$$

Similar to (25), we can write

$$\theta_\beta \overline{\frac{\partial V_{\beta_j}}{\partial x_k}}^{\beta} = \frac{\partial}{\partial x_k}(\theta_\beta V_{r\beta_j}) + \theta_\beta \frac{\partial \overline{V_{s_j}}^{s}}{\partial x_k}. \tag{52}$$

In view of (48), (51) and (52) we write (46) in the form

$$-\frac{1}{U_0}\int_{S_{s\beta}} \overset{\circ}{x}_i \rho_\beta V_{\beta_k}\frac{\partial V_{\beta_j}}{\partial x_k}\xi_{\beta_j}\, \mathrm{d}S$$

$$\cong \frac{c_{s\beta}}{2\Delta^2_{s\beta}}\overline{\rho_\beta}^{\beta}\tilde{F}^{s\beta}_{ijk} V_{r\beta_k} V_{r\beta_j} - \overline{\rho_\beta}^{\beta}\,\overline{V_{s_k}}^{s}\left[\frac{\partial}{\partial x_k}(\theta_\beta V_{r\beta_j}) + \theta_\beta \frac{\partial \overline{V_{s_j}}^{s}}{\partial x_k}\right](\delta_{ij} - T^{*}_{\beta_{ij}}). \tag{53}$$

Note that the second RHS term in (53) can be neglected if we assume that $\overline{\mathbf{V}}^{s}_{s} \ll \overline{\mathbf{V}}^{f}_{f}$.

Pressure gradients and Forchheimer terms expressing the exchange between the phases through their interfaces, govern the change in the wave velocity and its amplitude. Forchheimer terms may be regarded as source terms coupling between the solid and fluid momentum and energy balance equations. The coupling of these equations dictates the simultaneous change in the fluids inertia via changes in pressure gradient and Forchheimer's terms. The first affects the solid matrix effective stress towards equalization between the solid and fluids stresses. The second provides a mechanism for shifting momentum flux from the fluids to the solids, towards equalization between solid and fluid velocities. This, in turn, results in changes in the solid inertia.

In what follows, we will describe the roll of Forchheimer terms by comparing shock tube experiments and numerical simulation of compaction waves traveling through a 1-D saturated thermoelastic porous medium.

From hereafter we will refer to the macroscopic equations and, accordingly, will omit the $\overline{(\,)}^{\alpha}$ (or the $\overline{(\,)}^{\beta}$) designators.

4. Compaction waves in a 1-D saturated thermoelastic porous medium

Following the abrupt onset of the fluid's pressure and temperature, Levy et al. (1995) provided a dimensional analysis of the phases macroscopic balance equations, presented in the previous section. This analysis yielded four evolution periods (time intervals) associated with different dominant balance equations for the fluid and solid phases. During the second time interval, compaction wave equations were formed. The 1-D compaction wave equations resulting from (6–9, 14, 15) balance equations (Levy et al., 1996) when written in a vector form (using new variables) are as follows,

$$\frac{\partial \mathbf{U}}{\partial t}+\frac{\partial \mathbf{F}}{\partial x}=\mathbf{Q}. \tag{54}$$

The variable vector, $\mathbf{U}$, is defined by

$$\mathbf{U}=[r_{\mathrm{f}}, r_{\mathrm{s}}, m_{\mathrm{f}}, m_{\mathrm{s}}, E_{\mathrm{f}}, E_{\mathrm{s}}]^{\mathrm{T}} \tag{55}$$

where

$$\begin{aligned} &r_{\mathrm{f}}\equiv\phi\rho_{\mathrm{f}} \quad m_{\mathrm{f}}\equiv r_{\mathrm{f}}V_{\mathrm{f}} \quad E_{\mathrm{f}}\equiv r_{\mathrm{f}}e_{\mathrm{f}}=r_{\mathrm{f}}\left(C_{\mathrm{f}}T_{\mathrm{f}}+\frac{V_{\mathrm{f}}^2}{2}\right),\\ &r_{\mathrm{s}}\equiv(1-\phi)\rho_{\mathrm{s}} \quad m_{\mathrm{s}}\equiv r_{\mathrm{s}}V_{\mathrm{s}} \quad E_{\mathrm{s}}\equiv r_{\mathrm{s}}e_{\mathrm{s}}=r_{\mathrm{s}}\left(C_{\mathrm{s}}T_{\mathrm{s}}+\frac{V_{\mathrm{s}}^2}{2}\right). \end{aligned} \tag{56}$$

e_{α} denotes the total energy per mass unit of the α phase.

The flux vector, $\mathbf{F}$, is given by

$$\mathbf{F}=\begin{bmatrix} m_{\mathrm{f}} \\ \dfrac{m_{\mathrm{f}}^2}{r_{\mathrm{f}}}+T_{\mathrm{f}}^{*}\phi P \\ \dfrac{m_{\mathrm{s}}^2}{r_{\mathrm{s}}}-\sigma_{\mathrm{s}}'+(1-\phi T_{\mathrm{f}}^{*})P \\ \dfrac{m_{\mathrm{f}}}{r_{\mathrm{f}}}(E_{\mathrm{f}}+T_{\mathrm{f}}^{*}\phi P) \\ \dfrac{m_{\mathrm{s}}}{r_{\mathrm{s}}}(E_{\mathrm{s}}-\sigma_{\mathrm{s}}'+(1-\phi T_{\mathrm{f}}^{*})P) \end{bmatrix}. \tag{57}$$

The source vector, $\mathbf{Q}$, is given by

$$\mathbf{Q}=\begin{bmatrix} 0 \\ 0 \\ T_{\mathrm{f}}^{*}P\dfrac{\partial\phi}{\partial x}-\tilde{F}r_{\mathrm{f}}\left|\dfrac{m_{\mathrm{f}}}{r_{\mathrm{f}}}-\dfrac{m_{\mathrm{s}}}{r_{\mathrm{s}}}\right|\left(\dfrac{m_{\mathrm{f}}}{r_{\mathrm{f}}}-\dfrac{m_{\mathrm{s}}}{r_{\mathrm{s}}}\right) \\ -T_{\mathrm{f}}^{*}P\dfrac{\partial\phi}{\partial x}+\tilde{F}r_{\mathrm{f}}\left|\dfrac{m_{\mathrm{f}}}{r_{\mathrm{f}}}-\dfrac{m_{\mathrm{s}}}{r_{\mathrm{s}}}\right|\left(\dfrac{m_{\mathrm{f}}}{r_{\mathrm{f}}}-\dfrac{m_{\mathrm{s}}}{r_{\mathrm{s}}}\right) \\ \dfrac{m_{\mathrm{s}}}{r_{\mathrm{s}}}\left[T_{\mathrm{f}}^{*}P\dfrac{\partial\phi}{\partial x}-\tilde{F}r_{\mathrm{f}}\left|\dfrac{m_{\mathrm{f}}}{r_{\mathrm{f}}}-\dfrac{m_{\mathrm{s}}}{r_{\mathrm{s}}}\right|\left(\dfrac{m_{\mathrm{f}}}{r_{\mathrm{f}}}-\dfrac{m_{\mathrm{s}}}{r_{\mathrm{s}}}\right)\right] \\ \dfrac{m_{\mathrm{s}}}{r_{\mathrm{s}}}\left[-T_{\mathrm{f}}^{*}\dfrac{\partial\phi}{\partial x}+\tilde{F}r_{\mathrm{f}}\left|\dfrac{m_{\mathrm{f}}}{r_{\mathrm{f}}}-\dfrac{m_{\mathrm{s}}}{r_{\mathrm{s}}}\right|\left(\dfrac{m_{\mathrm{f}}}{r_{\mathrm{f}}}-\dfrac{m_{\mathrm{s}}}{r_{\mathrm{s}}}\right)\right] \end{bmatrix} \tag{58}$$

in which $\tilde{F}$ denotes the Forchheimer coefficient for an isotropic solid matrix. The pressure P, is prescribed by the equation of state,

$$\phi P=(\gamma-1)\left(E_{\mathrm{f}}-\frac{m_{\mathrm{f}}^{2}}{2r_{\mathrm{f}}}\right) \tag{59}$$

where γ denotes the specific heat capacities ratio of the fluid phase.

In view of (13) we can express the constitutive relation for the effective stress σ_{s}', in the form

$$\sigma_{\mathrm{s}}'=E_{\varepsilon}\varepsilon_{\mathrm{sk}}-E_{\mathrm{T}}C_{\mathrm{s}}(T_{\mathrm{s}}-T_{\mathrm{s0}}) \tag{60}$$

in which E_{ε} ($\equiv\lambda_{\mathrm{s}}''+\mu_{\mathrm{s}}'$) and E_{T} ($\equiv\eta/C_{\mathrm{s}}$) are the one dimensional macroscopic Lame coefficients for a thermoelastic solid. The porosity, ϕ, and the skeleton strain, $\varepsilon_{\mathrm{sk}}$, can be expressed as,

$$\begin{aligned} \phi &= 1-r_{\mathrm{s}}/\rho_{\mathrm{s}}, \\ \varepsilon_{\mathrm{sk}} &= 1-r_{\mathrm{s}}/r_{\mathrm{s0}}. \end{aligned} \tag{61}$$

Hence, the effective stress, σ_{s}', can be rewritten to read

$$\sigma_{\mathrm{s}}'=E_{\mathrm{c}}\left(\frac{r_{\mathrm{s0}}-r_{\mathrm{s}}}{r_{\mathrm{s0}}}\right)-E_{\mathrm{T}}\left(\frac{E_{\mathrm{s}}}{r_{\mathrm{s}}}-\frac{E_{\mathrm{s0}}}{r_{\mathrm{s0}}}-\frac{m_{\mathrm{s}}^{2}}{2r_{\mathrm{s}}^{2}}+\frac{m_{\mathrm{s0}}^{2}}{2r_{\mathrm{s0}}^{2}}\right) \tag{62}$$

where, the subscript $(\,)_{\mathrm{s}_0}$ denotes the solid properties at an initial state.

The set (54) of six partial differential governing equations defined by (55), (57) and (58) are to be solved for six unknowns namely; r_{f}, r_{s}, m_{f}, m_{s}, E_{f} and E_{s}. Consequently, in principle, given the apropriate conditions, the set is complete and can be solved. However, due to the complexity of the equations, an analytical solution of the set is not feasable. Instead, a numerical solution has been performed.

Note that in writing (54) we assumed that the gradients of the porosity were very small and therefor they might be written as source terms in the source vector, $\mathbf{Q}$, given by (58). As a result, the source vector, $\mathbf{Q}$, contains derivative terms and thus affects the character of the

equations (hyperbolic rather then elliptic–hyperbolic). This is very convenient for numerical purposes and is correct only when the gradients of the porosity are very small as is the case in this study. Applying this procedure removes the ill-posedness associated with the elliptic–hyperbolic character of the equations which is usually manifested in highly oscillatory solutions as the mesh is refined.

The numerical scheme for solving (54) is reported in Levy (1995) and Levy et al. (1996). It is based on an upwind TVD shock-capturing scheme, originally developed by Harten (1983), which was extended to solve the problem of compaction waves propagation in saturated thermoelastic porous media.

5. Comparison between the numerical predictions and the experimental results

In order to validate the physical model and the numerical code, the governing equations were solved numerically for different samples and a variety of initial conditions and compared to experimental results. In order to solve the governing equations and compare the solution to the experimental results, the various parameters which appear in the physical model, namely: the macroscopic Lame coefficients for a thermoelastic solid, E_ε and E_T, the Forchhiemer factor, $\tilde{F}$, the fluid tortuosity, T_f^*, and the intrinsic density of the solid matrix, ρ_s, which appear in the physical model, had to be estimated for each sample. Based on the properties of the materials of which the samples were made and the fact that the upper limit of the elastic stress reduces when the porosity increases, in a $(1-\phi)^2$ manner, (Gibson and Ashby, 1988) the magnitudes of the macroscopic Lame coefficients, E_ε and E_T, were estimated to be identical for all the samples, $E_\varepsilon = 380 \times 10^7$ Pa and $E_T = 26.207$ Kg/m^3.

The sensitivity of the predictions of the numerical code to these coefficients will be reported in a future study. The intrinsic density of the solid matrix for all the samples (silicon carbide, SiC, and alumina, Al_2O_3), as provided by the manufacturer, was $\rho_s = 2000 \pm 60$ Kg/m^3.

The tortuosity factors, T_f^* for the various samples were found by estimating the ratio between the speed of sound of the air inside the porous medium a_f and that in pure air a (Li et al., 1995),

$$\left(\frac{a_f}{a}\right)^2 = \frac{(1 - T_f^* + \gamma T_f^*)T_f^*}{\gamma}. \tag{63}$$

The Forchheimer factors, $\tilde{F}$, for the various samples where found experimentally. In these experiments, each sample was mounted in a pipe and the pressure drop across it was measured as a function of the air flow rate. The pressure drop was found to be a parabolic function of the air velocity. This was done by assuming that the pressure drop depends linearly on the length of the sample. The values of the tortuosity and the Forchhiemer factors, as obtained experimentally for the various samples, are presented in Table 1.

In order to validate the physical model, (54) was solved numerically, for different samples and initial conditions, and compared to experimental results. Table 2 represents the initial conditions of 18 different experiments. The comparison between the predictions of the numerical simulations and the experimental results, for all the cases appearing in Table 2, are

Table 1
The Forchheimer and the tortuosity factors, porosity and sample length for the different samples

The sample material	Sample type	Pores per inch (ppi)	$\tilde{F}$ (1/m)	T_f^*	ϕ	Sample length (mm)
Silicon carbide	I	10	300	0.7	0.728 ± 0.016	40, 60, 81
(SiC)	II	20	500	0.7	0.745 ± 0.001	41, 62, 83
Alumina	III	30	900	0.75	0.814 ± 0.010	48, 93
(Al_2O_3)	IV	40	1800	0.75	0.821 ± 0.007	50, 99

given in Levy (1995). In what follows, we will present two of these comparisons the experiments of which are listed in Table 2 as test numbers 1 and 13.

Fig. 1(a)–(e) and 2(a)–(e) represent typical experimental results and their numerical simulations for SiC and Al_2O_3 samples, respectively. P_1 is the pressure ahead of both the incident and the transmitted shock waves, P_2 is the theoretical pressure which should have been reached behind the incident shock wave, and P_5 is the theoretical pressure which should have been reached had the incident shock wave reflected head-on from a solid surface. The symbols represent the experimental results, the solid lines are the numerically predicted values when accounting for Forchheimer terms and the dash-dot lines represent the simulations without Forchheimer terms. The pressure histories of the pure gas just ahead of the front edge of the porous sample are shown in Fig. 1(a) and (b) for the SiC and 2(a) for the Al_2O_3. The pressure histories of the gas occupying the pores of the porous material along the shock tube side-wall and at its end-wall are shown in Fig. 1(c)–(e) for the SiC samples and 2(a)–(e) for the

Table 2
The initial conditions for the various experiments

Test number	Sample material	Sample length (mm)	Initial pressure (KPa)	Initial temperature (K)	Shock Mach number—M_i
1		40	83.04	290.0	1.378
2	SiC	60	83.11	290.5	1.385
3		81	83.41	290.5	1.377
4	10 ppi	81	83.71	289.5	1.543
5		81	83.70	290.5	1.734
11		48	82.84	292.0	1.374
12	Al_2O_3	93	83.41	290.5	1.377
13	30 ppi	93	83.36	291.0	1.539
14		93	83.12	291.5	1.744
15		50	83.09	292.0	1.374
16	Al_2O_3	50	83.08	292.5	1.545
17	40 ppi	50	83.10	292.5	1.741
18		99	83.16	290.5	1.377

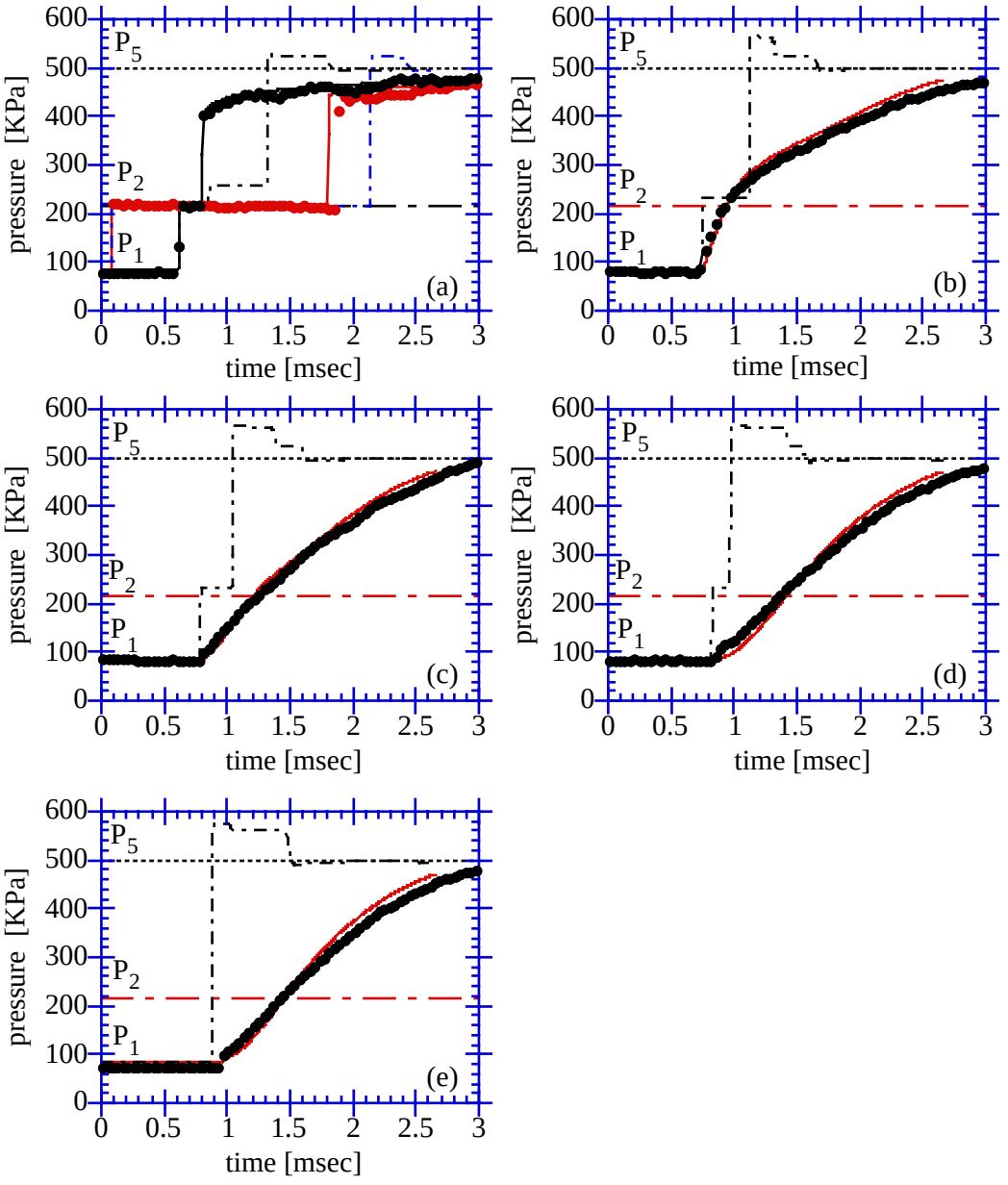

Fig. 1. Typical experimental results and their numerical simulations with a 40 mm long sample made of SiC having 10 pores per inch (sample I in Table 1). The incident shock wave Mach number in this experiment was $M_i = 1.378$ (test number 1 in Table 2). The pressure histories of the pure gas just ahead of the front edge of the porous material are shown in Fig. 1(a) and 2(b). The pressure histories of the gas occupying the pores of the porous material along the shock tube side-wall and at its end-wall are shown in Fig. 1(c)–(e), respectively. The symbols represent the experimental results, the solid lines are the numerically predicted values when accounting for Forchheimer terms and the dash–dot lines represent the simulations without Forchheimer terms. P_1 is the pressure ahead of both the incident and the transmitted shock waves, P_2 is the theoretical pressure which should have been reached behind the incident shock wave, and P_5 is the theoretical pressure which would have been reached had the incident shock wave reflected head-on from a solid end-wall.

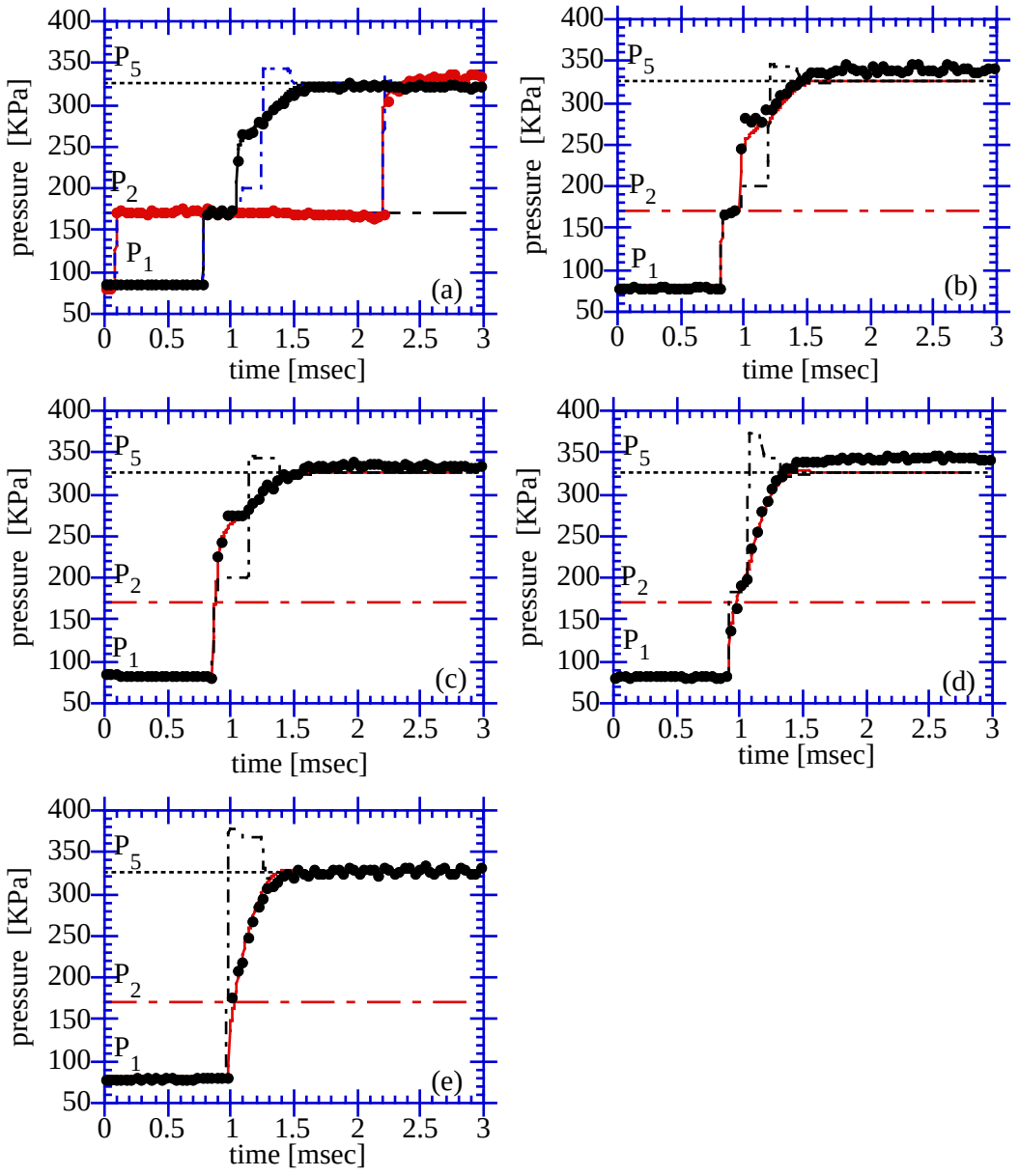

Fig. 2. Typical experimental results and their numerical simulations with a 93 mm long sample made of Al_2O_3 having 30 pores per inch (sample III in Table 1). The incident shock wave Mach number in this experiment was $M_i = 1.539$ (test number 13 in Table 2). The pressure histories of the pure gas just ahead of the front edge of the porous material are shown in Fig. 2(a). The pressure histories of the gas occupying the pores of the porous material along the shock tube side-wall and at its end-wall are shown in Fig. 2(b)–(e), respectively. The symbols represent the experimental results, the solid lines are the numerically predicted values when accounting for Forchheimer terms and the dash–dot lines represent the simulations without Forchheimer terms. P_1, P_2, and P_5 are defined in the caption of Fig. 1.

Al_2O_3 samples. Figs. 1 and 2, clearly emphasize the advantage of simulations with Forchheimer terms in retrieving the experimental observations. Major differences between the two cases are evident. While the simulations without Forchheimer terms, (dashed doted lines) do not agree with the experimental results, simulations with Forchheimer terms (solid lines) results in predictions which excellently reproduce the experiments. When Forchheimer terms are neglected, the shock waves which are refelected, head-on, from the front edge of the porous sample, are weaker than those obtained when the Forchheimer terms are accounted for [compare the second jump in the pressure traces shown in Fig. 1(a), (b) and 2(a)]. These figures also indicate that when the Forchheimer terms are neglected, a sharp shock wave is transmitted at a later time from the porous material into the gaseous phase resulting in a third jump in pressure longer than P_5. These high pressures are later decayed by the transmitted expansion waves and reach, as expected, the value of P_5. In addition, as a result of the neglection of the Forchheimer terms, the shock waves which are transmitted into the porous material samples do not develop a dispersed structure, as is the situation in reality. Instead, they maintain their sharp fronts. The fact that the transmitted shock waves maintain their sharp structure results in a jump to pressures larger than P_2 behind them [see the sharp jumps in the pressures inside the porous samples in Fig. 1(c), (d), 2(c), (d)]. Fig. 1(e) and 2(e) in which the pressure histories at the back edge of the porous samples (i.e. at the shock tube end-wall) are shown again, indicate that when the Forchheimer terms are neglected, in contrast to the experimental results, sharp shock waves reach the end-wall. The reason for the above mentioned differences lies in the fact that the Forchheimer terms emphasize the friction between the two phases and, as a result, increase the rate of momentume exchange. This in turn results in a situation in which much larger impulses, $\int P\,\mathrm{d}t$, are predicted numerically when the Forchheimer terms are neglected.

It is clearly evident from these comparisons that the agreement between the experimental results and the numerical predictions is very good. Note that there are disagreements between the numerical and the experimental positions of the reflected shock wave after it traveled a relatively long distance from the front edges of the samples [see Fig. 1(a) and 2(a)]. The agreement regarding the reflected shock wave position was better in the case of low incident shock wave Mach numbers and short samples. This may be caused by the way the porosity gradient terms were treated in the source vector, $\mathbf{Q}$.

Although Fig. 1(a)–(e) and 2(a)–(e) describe the results of only two typical experiments, one in the silicon-carbide (SiC) sample and one in an alumina (Al_2O_3) sample, similar good to excellent agreements were obtained in the comparisons with all the experiments which were conducted in the course of the present study (Levy, 1995).

It should be noted that there are two types of transversal waves which propagate in porous media. The reason for this is the different compressibility of the porous skeleton and the fluid which saturates it. They are known as "fast" and "slow" waves. The fast wave, i.e. the compaction wave, propagates through the skeleton and the slow one, i.e. the transmitted wave, through the fluid occupying the pores. When the values of the compressibility are very different, as is the case in this study, the amplitudes of these two waves are very different and hence the influence of the fast wave on the fluid cannot be observed. For this reason the fast wave is not evident in Figs. 1 and 2 where the fluid pressure is shown. Had the solid stress been presented, both waves would have been recorded as was shown by Levy et al.

(1997). Hence, the analytical model and the computer code presented and used in this study are, in fact, capable of reproducing both the fast and the slow waves.

6. Conclusions

Macroscopic balance equations of mass and momentum are described for the case of multiphase porous media. To these, we add the energy balance equation when considering the case of saturated thermoelastic porous media.

For both cases, we show that microscopic terms of inertia should be accounted for at the interfaces between the solid phase and the fluid phases. These microscopic terms are then developd into macroscopic ones by rigorous mathematical evaluations leading to Forchheimer terms. The macroscopic terms represent sources of momentum and energy that are exchanged between the fluid phases and the solid phase, at their solid–fluid interfaces.

Numerical simulations of compaction waves in a 1-D saturated porous medium, were compared with shock tube experiments. These simulations were done with and without Forchheimer terms. The case of accounting for Forchheimer terms demonstrates almost no deviation from experimental results and was, by far, better then the case when we did not include these terms.

References

Bear, J., Bachmat, Y., 1990. Introduction to Modeling of Transport Phenomena in Porous Media. Kluwer, Dordrecht.

Bear, J., Sorek, S., 1990. Evolution of governing mass and momentum balance equations following an abrupt pressure impact in a porous medium. Transp. Porous Media 5, 169–185.

Bear, J., Sorek, S., Ben-Dor, G., Mazor, G., 1992. Displacement waves in saturated thermoelastic porous media, I, basic equations. Fluid Dyn. Res. 9, 155–164.

Gibson, L.J., Ashby, M. F., 1988. Cellular solids—Structure and Properties. Program Press, Oxford.

Harten, A., 1983. High resolution schemes for hyperbolic conservation laws. J. Comput. Phys. 49, 357–393.

Hsu, C.T., Cheng, P., 1990. Thermal dispersion in a porous medium. Int. J. Heat Mass Transfer 33 (8), 1587–1597.

Levy, A., 1995. Wave propagation in a saturated porous media. Ph. D thesis. Department of Mechanical Engineering, Ben-Gurion University of the Negev, Beer Sheva, Israel.

Levy, A., Sorek, S., Ben-Dor, G., Bear, J., 1995. Evolution of the balance equations in saturated thermoelastic porous media following abrupt simultaneous changes in pressure and temperature. Transp. Porous Media 21, 241–268.

Levy, A., Ben-Dor, G., Sorek, S., 1996. Numerical investigation of the propagation of shock waves in rigid porous materials: development of the computer code and comparison with experimental results. J. Fluid Mech. 324, 163–179.

Levy, A., Ben-Dor, G., Sorek, S., 1997. Numerical investigation of the propagation of shock waves in rigid porous materials—solution of the Riemann problem. Int. J. Num. Meth. Heat Fluid Flow 7 (8), 801–813.

Li, H., Levy, A., Ben-Dor, G., 1995. Analytical prediction of regular reflection over porous surfaces and comparison with experiments. J. Fluid Mech. 282, 219–232.

Mei, C.C., Auriault, J.L., 1991. The effect of weak interia on flow through a porous medium. J. Fluid Mech. 222, 647–663.

Nikolaevskij, V.M., 1990. Mechanics of Porous and Fractured Media. World Scientific, Singapore.

Nield, D.A., 1991. The limitations of the brinkman–forchheimer equation in modelling flow in a saturated porous medium and at an interface. Int. J. Heat Fluid Flow 12, 269–272.

Nield, D.A., 1994. Modelling high speed flow of compressible fluid in a saturated porous medium. Transp. Porous Media. 14, 85–88.

Olim, M., van Dongen, M.E.W., Kitamura, T., Takayama, K., 1994. Numerical simulation of the propagation of shock waves in compressible open-cell porous foams. Int. J. Multiphase Flow 20 (3), 557–568.

Sorek, S., Bear, J., Ben-Dor, G., Mazor, G., 1992. Shock waves in saturated thermoelastic porous media. Transp. Porous Media 9, 3–13.

Tiziana, G., 1997. Derivation of the Forchheimer law via matched asymptotic expansions. Transp. Porous Media 29, 191–206.

Whitaker, S., 1996. The Forchheimer equation: a theoretical development. Transp. Porous Media 25, 27–61.

Wodie, J.C., Levy, T., 1991. Correction non lineaire de la loi de Darcy. C. R. Acad. Sci., Paris t. 312, Serie II , 157–161.